On the collision rate of small particles in isotropic turbulence. I. Zero-inertia case

Lian-Ping Wang,[a] Anthony S. Wexler, and Yong Zhou
Department of Mechanical Engineering, 126 Spencer Laboratory, University of Delaware, Newark, Delaware 19716-3140

Numerical experiments have been performed to study the geometric collision rate of finite-size particles with zero inertia (i.e., fluid elements) in isotropic turbulence. The turbulent flow was generated by the pseudospectral method. We argue that the formulation of Saffman and Turner [J. Fluid Mech. **1**, 16 (1956)] for the average collision kernel is correct only under the assumptions that the particles are kept in the system after collision and allowed to overlap in space. This was confirmed, for the first time, by numerical experiments to within a numerical uncertainty as small as 1%. Finite corrections to the Saffman and Turner result must be made if one applies the theory to actual coagulation process where particles are not allowed to overlap before collision and particles are removed from a given size group after collision. This is due to the fact that Saffman and Turner assumed a *uniform, time-independent concentration field* in their formulation of the average collision kernel, while in the actual modeling of population evolution the particle number concentration *changes in time* and may be *locally nonuniform* as a result of a biased removal process due to spatially nonuniform coagulation rates. However, the quantitative level of the deviations from the Saffman and Turner result remain to be explained. Numerical experiments in simple shear flow were also conducted to elaborate our findings. © *1998 American Institute of Physics.* [S1070-6631(98)00901-5]

I. INTRODUCTION

The rate of coagulation in turbulent dispersions of small solid particles and droplets is important to many areas of meteorology and engineering. In the atmosphere it contributes to precipitation and cloud processing of aerosols. To a wide variety of technologies in chemical and energy industries, formation of particle clusters due to coagulation has a profound effect on the stability of dispersions, the quality of dried products, and the efficiency of energy conversion. The wide range of applications include modeling of cloud microphysical processes, production of titanium-dioxide pigments, design of fine spray combustion nozzles and gas cleaning equipment, and control of industrial emissions. In these applications, we wish to develop an accurate model, or population balance equations, for the time evolution of the size distribution of the particles for which turbulent coagulation is a key physical process.

The overall coagulation rate of finite-size particles in fluid turbulence is governed by three consecutive and interrelated processes: (1) geometric collision due to particle–turbulence interactions, (2) collision efficiency due to local particle–particle aerodynamic interactions, and (3) coagulation efficiency as determined by surface sticking characteristics. We focus here on the geometric collision rate, which describes the rate of geometric overlaps among particles due to turbulent transport.

In this paper we consider the geometric collision of monodisperse particles, however, results to be presented can be extended to polydisperse system. We shall assume that the particles are small in size, typically on the order of the flow Kolmogorov length scale $\eta = (\nu^3/\bar{\epsilon})^{1/4}$, where ν and $\bar{\epsilon}$ are fluid kinematic viscosity and the average rate of energy dissipation per unit mass, respectively. In addition, the particle inertial response time $\tau_p = \rho_p d_p^2/(18\rho\nu)$ is much smaller than the flow Kolmogorov time scale $\tau_K = (\nu/\bar{\epsilon})^{1/2}$, so that the particles follow the local fluid motion precisely. Here d_p and ρ_p are particle diameter and density; ρ is fluid density. The zero-inertia assumption is only valid when the turbulence dissipation rate $\bar{\epsilon}$ is not very large (such as in stratiform clouds and small cumulus clouds) and the particle size is sufficiently small. Our purpose is to critically examine the classical result on the average collision kernel for zero-inertia particles obtained by Saffman and Turner[1] in 1956 (also the 1988 Corrigendum; hereafter will be referred to as ST).

Consider a monodisperse system consisting of N_p particles in a volume Ω, the collision rate per unit volume, $\dot{\mathcal{N}}_c$, is written as

$$\dot{\mathcal{N}}_c = \Gamma \frac{\bar{n}^2}{2}, \tag{1}$$

provided that $N_p \gg 1$, where $\bar{n} \equiv N_p/\Omega$ is the average particle number concentration in the volume and Γ is the collision kernel. For zero-inertia particles, Saffman and Turner[1] showed that

$$\Gamma = 2\pi R^2 \overline{|w_r|}, \tag{2}$$

where R is the geometric collision radius, the distance at which two particles start to touch each other, and is equal to d_p for a monodisperse system. Here $\overline{|w_r|}$ is the average rela-

[a] Corresponding author: Department of Mechanical Engineering, 126 Spencer Laboratory, University of Delaware, Newark, Delaware 19716-3140. Phone: (302) 831-8160; Fax (302) 831-3619; Electronic mail: LWANG@ME.UDEL.EDU

tive velocity in the longitudinal direction between two points separated by a distance R. An underlying assumption in (2) is that the particle concentration field is uniform in space, so that the overbar in (2) denotes an ensemble or spatial average in homogeneous turbulence. If, on the other hand, the particle concentration is nonuniform, the effect of concentration variation must be taken into account in the definition of the average collision kernel. In other words, the average for the relative velocity should be weighted with the particle concentration field.

After further assuming that, $R \ll \eta$, the turbulent flow is locally isotropic, and the probability distribution of the velocity gradient is Gaussian, Saffman and Turner[1] gave the following expression for Γ:

$$\Gamma = 1.294 R^3 \left(\frac{\bar{\epsilon}}{\nu} \right)^{1/2}. \tag{3}$$

Using a more accurate lognormal distribution for the velocity gradient, Balachandar[2] showed that the coefficient in (3) would be increased slightly, depending on the flatness factor of the velocity gradient. It should be noted that Eq. (2), in principle, can be used even for $R > \eta$ if the relative velocity can be related to R and turbulence parameters. Delichatsios and Probstein,[3] for example, used Eq. (2) for R in the inertial subrange. Therefore, Eq. (2) is much more general than Eq. (3).

The ST results are viewed to be more rigorous than the earlier result by Camp and Stein,[4] who first applied the theory of Smoluchowski[5] for simple shear flow to turbulence. Although Eqs. (2) and (3) have been widely cited and used in the literature, they have never been confirmed directly. We note that Saffman and Turner derived Eq. (2) by considering a *uniform, time-independent concentration field* in which particles could overlap if distributed randomly. The result, Eq. (2), was formulated before they studied the population evolution later in their paper in which the concentration *changed in time* and might be *locally nonuniform* as a result of a biased removal process due to spatially nonuniform local coagulation rates (See Sec. IV C). Therefore, there is an inconsistency in the ST work when their result is applied to the actual coagulation process. The main purpose of our paper is to clarify the effect of this inconsistency on the exact value of the collision kernel when the particles are either not allowed to overlap or removed as a result of collisions.

Equation (3), apart from the coefficient 1.294, must be correct for $R \ll \eta$ as it can be derived simply from a dimensional analysis.[6] Similar expressions with different coefficients are found in the literature.[3,4,7,8] Recent numerical simulations[2,9] also showed a slightly different collision kernel than (3). We will demonstrate that Eq. (2) [and (3) if the Gaussian distribution is a good approximation for the flow field and $R < \eta$] correctly describes the collision rate of zero-inertia particles, under the assumptions that the particles are kept in the system after collision and are allowed to overlap in space. Finite corrections to the ST result are needed, depending on the details of the collision detection.

It should be noted that several attempts had been taken to measure the collision kernel directly.[3,8,10,11] However, it is very difficult to perform well-controlled experiments in which one can isolate one collision mechanism from others (say, shear-induced collision from Brownian coagulation, geometric collision from hydrodynamic interactions). On the other hand, numerical simulations can be used to study one mechanism at a time and have recently been used to derive the collision kernel for both buoyant and heavy particles.[2,9,12–14] In this paper we will use numerical simulations to provide information necessary to clarify existing theory for zero-inertia particles. In part 2 of this work,[6] we apply similar numerical experiments to particles with finite inertia. We use turbulent flow fields generated by numerically integrating the full Navier–Stokes equations directly. By this means, local flow dynamic features are represented without any *ad hoc* modeling.

The paper is organized as follows. In the next section we provide the details of the flow simulation, particle tracking, and collision detection. In Sec. III, we describe numerical simulation results in a frozen turbulence and compares them to the ST theory. A close examination of the ST theory is presented in Sec. IV in light of numerical results. The results for an evolving turbulence are given in Sec. V. Finally main conclusions are summarized in Sec. VI.

II. NUMERICAL SIMULATION

A. Flow field

A homogeneous and isotropic turbulent flow was generated by full numerical simulations using a pseudospectral method. The spectral code was originally developed by Ruetsch and Maxey[15] and was used as a basis for the study of particle settling and concentration field by Wang and Maxey.[16] The incompressible Navier–Stokes equations,

$$\frac{\partial \mathbf{u}}{\partial t} = \mathbf{u} \times \vec{\omega} - \nabla \left(\frac{P}{\rho} + \frac{1}{2} \mathbf{u}^2 \right) + \nu \nabla^2 \mathbf{u} + \mathbf{f}(\mathbf{x}, t), \tag{4}$$

were solved along with the continuity equation $\nabla \cdot \mathbf{u} = 0$ in a periodic box of side $L = 2\pi$. Here $\vec{\omega} \equiv \nabla \times \mathbf{u}$ is the vorticity and P is the pressure. The flow domain is discretized uniformly into N^3 grid points, which defines the wave number components in Fourier space as $k_j = \pm n_j (2\pi/L)$, where $n_j = 0, 1, ..., 1/2N$ for $j = 1, 2, 3$. A small portion of the energy in the higher wave numbers, $|\mathbf{k}| \geq 1/2N - 1.5$, is truncated at each time step to reduce aliasing errors, so the highest wave number realized in our simulation is $k_{max} = 1/2N - 1.5$. The time evolution is computed by applying a second-order Adams–Bashforth scheme to the nonlinear terms, a second-order Crank–Nicholson scheme for the viscous terms, and the Euler scheme for the random forcing term. The pressure is eliminated through the continuity equation.

The flow was generated from rest by the random forcing term $\mathbf{f}(\mathbf{x}, t)$, which was nonzero only at low wave numbers, $|\mathbf{k}| < \sqrt{8}$, following the forcing scheme developed by Eswaran and Pope.[17] In this scheme the forcing term is specified as a complex, vector-valued Uhlenbeck–Ornstein (UO) stochastic process. The net rate of energy addition was specified by the amplitude and correlation time scale of the forcing, the values of which can be found in Wang and Maxey.[16] Nonlinear interactions propagate energy from low to high

wavenumbers and eventually viscous dissipation becomes active, leading to a quasisteady balance of the forcing energy and the viscous dissipation. In addition to the grid resolution and the forcing parameters, the only remaining physical parameter that needs to be specified for the flow simulation is the kinematic viscosity ν. The spatial resolution of a spectral simulation is often monitored by the value of $k_{max}\eta$, which should be greater than unity for the smallest scales of the flow to be resolved (see, for example, Eswaran and Pope[17]). For the simulations in this study, $k_{max}\eta$ was about 1.30. The time step was chosen to ensure that the CFL number was 0.3 or less for numerical stability and accuracy.[17] Other details of the flow simulation can be found in Wang and Maxey.[16]

For most discussions in this paper, the flow was frozen after the statistically stationary stage was reached, and particles were then introduced into the flow. The start of particle release will be denoted as $t=0$. This provides us with an identical flow microstructure for different runs with various particle parameters and collision counting methods. It is also in the context of ST, as they essentially assumed a quasi-steady local straining flow field. The case of evolving flow will be briefly considered in Sec. V.

Since all the important flow scales are resolved in a full numerical simulation, the grid resolution determines the scale separation, and thus the Reynolds number of the resulting flow. For the purpose of this paper, we only use a low resolution flow at 32^3 with a Taylor microscale Reynolds number of 24. It should be noted that the flow Reynolds number is irrelevant as far as Eq. (2) is concerned. It can, however, alter the probability distribution of the velocity gradient and lead to a slightly different coefficient in (3). The important flow parameters are given here for later use: $\nu = 0.6$, $\bar{\epsilon} = 3569$, $\eta = 0.0882 = 0.45\,\Delta x$, $\tau_k = 0.013$, and the rms fluid fluctuating velocity $u' = 17.02$.

B. Particle motion

The particles are assumed to follow the local fluid motion. The location of a particle at time t, $\mathbf{Y}(t)$, is governed by

$$\frac{d\mathbf{Y}(t)}{dt} = \mathbf{u}[\mathbf{Y}(t),t], \tag{5}$$

where $\mathbf{u}(\mathbf{Y},t)$ is the fluid velocity at the particle location and was determined numerically from the values at neighboring grids using a six-point Lagrange interpolation. A fourth-order Adams–Bashforth method was used to advance the particle location. Typically, 10^3-10^4 particles were introduced at $t=0$ into the computational domain at random initial positions. The particle size was made as large as $\mathcal{O}(\eta)$ so that there were a significant number of collision events. The particle volume fraction was small, typically less than 5%.

C. Collision detection

1. Definition of collision

A careful definition of collisions is crucial to the implementation of a collision detection algorithm in a numerical simulation. We define a collision as an event when two particles are brought together from $d(t_1)>R$ to $d(t_2)\leq R$ with

$t_2>t_1$, where $d(t)$ is the separation distance from center to center at time t between two particles in a pair selected for collision detection. Therefore, collision detection is mainly done by computing $d(t)$.

In a numerical simulation, if the orbit of each particle is known exactly, $d(t)$ can be computed exactly for any time interval $t^{(n)}<t<t^{(n+1)}$ by interpolation. If the time step dt is small enough, we can trace each particle before and after a collision. However, in practice, we would like to choose dt as large as possible in order to save computer time, with the requirement that any particle does not participate in more than one collision in the time interval. Then care must be taken to prevent omissions in counting the collisions. For any given time interval, there are three situations when a *collision event* must be counted.

(i) If $d(t^{(n)})>R$ and $d(t^{(n+1)})\leq R$, a collision must occur and we shall refer to this collision as a type I collision.

(ii) If $d(t^{(n)})>R$ and $d(t^{(n+1)})>R$, a collision could occur in the time interval if $d(t)\leq R$ for $t^{(n)}<t<t^{(n+1)}$. We shall refer this type of collision as a type II collision.

(iii) If $d(t^{(n)})\leq R$ and $d(t^{(n+1)})\leq R$, the particle pair is already in contact at the beginning of the time step and is still in contact at the end of the time step. A collision event must be recorded if $d(t)>R$ for $t^{(n)}<t<t^{(n+1)}$. This will be refered to as a type III collision.

2. Collision detection algorithm

We basically followed the algorithm of Balachandar.[2] A primary detection grid of cell size W was introduced, along with a second grid of the same cell size but shifted in each direction by $W/2$. Each particle's location was identified first with a cell in the primary grid. The collision detection involving this selected particle was restricted to a neighborhood defined as the region formed by the eight cells in the second grid that overlapped with the cell in the primary grid where the particle was found. This method reduces dramatically the total number of pairs to be checked for possible collision within a given time step, by a factor of $[L_B/(2W)]^3$, where $L_B = 2\pi$ is the size of the computation box. Obviously the smaller the cell size W, the more efficient the method becomes. On the other hand, the cell size W has to be large enough so that no collision pair could be missed.

Assume that the probability distribution of the particle velocity is close to Gaussian, then 99.999 94% of the particles would have velocity magnitude in any direction below $5u'$. It is safe to assume that the relative velocity for any particle pair in any direction is less than $10u'$. To count collisions, the algorithm selects a particle, identifies the primary cell for this particle, and then checks for other particles in the same primary cell and in a neighborhood comprising a 1/2 cell width ($W/2$) surrounding the primary cell in all directions. Therefore the minimum distance between two particles that are not considered for a collision is $W/2$. The requirement to almost guarantee this particle pair will not collide in dt is $W/2>R+10u'\,dt$. Therefore we set the width of the detection grid to be

$$W>2\left(\frac{R}{\Delta x} + \frac{10u'\,dt}{\Delta x}\right)\Delta x, \tag{6}$$

Wang, Wexler, and Zhou

where Δx is the grid spacing for turbulence simulation. As an example, if $u'=17$, $dt=0.001$, $R/\Delta x=0.8$, $N=32$, the grid dimension for collision detection is INT $(L_B/W)=9$, which is computationally 91 times faster than considering all pairs.

In numerical implementation, a coarse check for no collision was first done if

$$d(t^{(n)}) > R + |\Delta \mathbf{Y}|_i + |\Delta \mathbf{Y}|_j, \tag{7}$$

to save time, where $|\Delta \mathbf{Y}|_i$ and $|\Delta \mathbf{Y}|_j$ were the distance traveled in the time interval by the two particles, respectively. The detection of the type I collision only requires the interparticle distances $d(t^{(n)})$ and $d(t^{(n+1)})$, while both type II and type III collisions require an accurate representation of $d(t)$ in the time interval. This information was furnished by interpolating the particle orbit in the time interval with a third-order polynomial, using the locations and velocities of each particle at $t^{(n)}$ and $t^{(n+1)}$. The total number of collisions in the time interval is the sum of the collision events of three types. Obviously, if dt is very small, type II and III collisions rarely occur and type I collision accounts for almost all the collision events.

3. Post-collision treatment and collision kernel

As noted before, a given number of particles were introduced into the flow with random initial locations. They were transported subsequently by the flow and each particle was assumed to move independently. Three different collision counting schemes were considered that led to different results of the numerical collision kernel.

Scheme 1. Particles were allowed to overlap in the system at the beginning of a time step and were not removed from the system after collision. All the three collision events described in Sec. II C 1 could occur and were summed to give the total collision count. This scheme appears to be irrelevant to reality, but, as we will show, gives a collision kernel consistent with the ST formulation. We wish to clarify the underlying assumptions in the ST formulation through such a hypothetical scheme.

Scheme 2. At the beginning of each time step, the overlapping particles were marked and excluded from the consideration of collision detection. Therefore, the actual number of particles used for collision detection was less than the total number of particles used and varied in time. Type III collisions were not possible in this scheme.

Scheme 3. Particles were removed immediately from the system when they collided in the system. As a result, the total number of particles considered in collision detection decreased with time and particles remaining in the system were nonoverlapping at the beginning of each time step.

Obviously, the differences lie in the questions of which subset of particles are used for collision detection and whether particles are dropped upon collision. The advantage of keeping all the particles in the system is that one has a statistically stationary particle system (in schemes 1 and 2) and more accurate results can be obtained for a given initial number of particles. Since in scheme 3 the particle system is not statistically stationary, care must be taken to properly interpret the results, as will be shown in Sec. IV C.

For each of the three schemes, one can define a local-in-time collision kernel for any time step dt as

$$\Gamma_i(t^{(n)}) = \frac{2\Omega N_c(t^{(n)} \rightarrow t^{(n+1)})}{dt[N_{pi}(t^{(n)})]^2}, \tag{8}$$

where $i=1$, 2, and 3 denotes the individual schemes, $N_c(t^{(n)} \rightarrow t^{(n+1)}) \approx \dot{\mathcal{N}}_c \Omega \, dt$ is the total collision count in the time step $t^{(n)} < t \leqslant t^{(n+1)}$, $N_{pi}(t^{(n)})$ is the total number of particles participated in the collision detection and is given for each scheme as

$$N_{pi}(t^{(n)}) = \begin{cases} N_p = \text{const}, & \text{for } i=1; \\ N_p - 2N_0(t^{(n)}), & \text{for } i=2; \\ N_p(t^{(n)}), & \text{for } i=3; \end{cases} \tag{9}$$

where $N_0(t^{(n)})$ is the number of overlapping pairs at $t^{(n)}$ in scheme 2, and $N_p(t^{(n)})$ is the number of particles left in the system in scheme 3. It is assumed that the particle volume fraction is very small so that binary collisions dominate in the collision process. These local-in-time collision kernels were quite *noisy* if N_p is not very large. They can be improved by averaging over different realizations of the turbulence field and initial particle locations. It should be noted that Eq. (8) is simply a rearrangement of Eq. (1), with the actual collision detection schemes clearly specified. Equation (8) serves as a basis for testing various detection schemes in direct numerical or physical experiments.

For the first two schemes, the stationarity property allows a further average over time to yield the final collision kernel $\langle \Gamma_i \rangle$. However, for the more realistic scheme 3, $\Gamma_3(t)$ will decrease in time and care must be taken in interpreting the average kernel $\langle \Gamma_3 \rangle$ (see Sec. IV C). We note that $\Gamma_3(t)/\Omega$ can also be viewed as the local slope of the $1/N_p(t)$ vs t curve since $dN_p(t) = -2N_c(t^{(n)} \rightarrow t^{(n+1)})$, and upon integration we have

$$\frac{1}{N_p(t^{(n+1)})} = \frac{1}{N_p(t^{(n)})} + \frac{\Gamma_3(t^{(n)})}{\Omega} \, dt. \tag{10}$$

The decrease of the local slope with time was evident in previous studies by Balachandar[2] and Hu and Mei,[9] but was not explained.

III. RESULTS FROM NUMERICAL EXPERIMENTS

We shall first present results from the numerical experiments and compare them with theoretical predictions by Smoluchowski[5] for simple shear flow and by ST for isotropic turbulence. We argue that the collision counting scheme 1 reproduces *exactly* the predictions while deviations must occur for the other two schemes.

A. Simple shear flow

We first performed numerical experiments in simple shear flow with a velocity field given as

$$u(x,y,z) = \gamma z, \quad v(x,y,z) = 0, \quad w(x,y,z) = 0, \tag{11}$$

where γ is the shear rate. These experiments serve two purposes. First, they provide a simple way to validate the collision detection algorithm. Second, they will help to illustrate an important consequence of a subtle difference between the

TABLE I. Collision kernel in simple shear flow.

	$\langle\Gamma\rangle$	$\langle\Gamma\rangle/\Gamma$, Eq. (13)
Scheme 1	0.2992 ± 0.0050	0.994 ± 0.017
Scheme 2	0.3181 ± 0.0070	1.057 ± 0.023
Scheme 3	0.3251 ± 0.0114	1.080 ± 0.038
Eq. (13)	0.3009	$\cdots$
Eq. (27)	0.3211	1.067

TABLE II. Collision kernel in frozen turbulence.

	$\langle\Gamma\rangle$	$\langle\Gamma\rangle/\Gamma$, Eq. (2)
Scheme 1	0.3724 ± 0.0034	1.010 ± 0.009
Scheme 2	0.3954 ± 0.0042	1.072 ± 0.011
Scheme 3	0.3097 ± 0.0062	0.840 ± 0.017
Eq. (2)	0.3688	$\cdots$
Eq. (3)	0.3868	1.049
Eq. (27)	0.3935	1.067

simple shear flow and the isotropic turbulence: in the former the straining field or local dissipation rate field is uniform, while it is nonuniform in the latter.

The exact expression for the collision kernel was derived by Smoluchowski[5] to be

$$\Gamma = \frac{4}{3}\,\gamma R^3, \tag{12}$$

with the assumption that particles are uniformly distributed in an infinite domain. The computation domain for the simulation is a finite cube of size 2π and periodicity in all the three directions allows the extension of the domain to infinity. However, the velocity field (11) is periodic in x and y only. To circumvent this problem, we only distribute particles in a domain $0<x<2\pi$, $0<y<2\pi$, $0.5\pi<z<1.5\pi$ with periodicity applied in x and y only. A boundary correction must be added to the average collision kernel in this domain with respect to (12) (see the Appendix),

$$\Gamma = \frac{4}{3}\,\gamma R^3\left(1 - \frac{3\pi}{16}\frac{R}{l}\right), \tag{13}$$

where $l=\pi$ is the domain size in the z direction.

The numerical experiment was done with $\gamma=60$, $R=0.8\times2\pi/32$, $N_p=1024$, and $dt=0.0004$. The particle volume fraction was 1.68%. Here 21 realizations of particle initial locations were used to reduce the numerical uncertainties. The implied boundary correction in (13) is about 3%.

The results for the average collision kernel along with the 95% numerical confidence intervals are given in Table I. The numerical confidence intervals were estimated based on the 21 realizations of the average collision kernels. It is clear that scheme 1 gives a collision kernel 0.6% less than the theory given by Eq. (13), with a numerical uncertainty of 1.7%. Schemes 2 and 3, however, overestimate Γ by about 6% and 8%, respectively. The origin for the larger numerical values will be explored in Sec. IV B. It should be noted that the numerical results in Table I were unchanged as we increased dt to 0.004.

B. Isotropic turbulence

Table II gives results for a typical numerical experiment in isotropic turbulence with $R=0.8\times2\pi/32$, $N_p=2048$, $dt=0.002$, and a total integration time $t=0.8$ (about ten large-scale eddy turnover times). Again 21 realizations of particle initial locations were used to evaluate the 95% numerical confidence intervals shown in Table II. Also provided are the prediction based on Eq. (2) with $\overline{|w_r|}$ computed directly from the given flow field (the overbar is taken as a usual spatial average), and the prediction by Eq. (3). Comparison between

the two predictions indicates that Eq. (3) overpredicts the kernel by about 4.9%, which involves about 0.8% overprediction due to the assumption $R\ll\eta$, i.e.,

$$\overline{|w_r|}\times1.008 = \frac{R}{3}\overline{\left(\left|\frac{\partial u}{\partial x}\right| + \left|\frac{\partial v}{\partial y}\right| + \left|\frac{\partial w}{\partial z}\right|\right)},$$
$$\text{for} \quad R=0.8\,\Delta x = 1.78\,\eta, \tag{14}$$

and 4.1% overprediction due to the Gaussian assumption. In the following, we will refer to the prediction of Eq. (2), $\Gamma=0.3688$, as the exact prediction of the theory.

We observe that scheme 1 gives almost the same value as the prediction, with a relative error of about 1%. We note that the 95% numerical confidence interval is equivalent to 1% of Γ. Therefore we can claim that $\langle\Gamma_1\rangle=\Gamma$. Scheme 2 overestimates the kernel by 7.2%. The most interesting result is that the average numerical kernel from scheme 3 is smaller than the theoretical value by about 16%, a result in striking contrast to the result in simple shear flow. This will be discussed further in Sec. IV C.

To further support the above observations, we performed a series of numerical experiments by varying either N_p or particle size R. The total integration time was set to $t=0.8$ with $dt=0.001$. Use of a smaller time step yielded essentially the same results. Figure 1 shows the average numerical collision kernels normalized by the ST prediction as a func-

FIG. 1. Numerical collision kernels, normalized by $\Gamma_0=2\pi R^2\overline{|w_r|}$, as a function of particle size or collision radius $R/\Delta x$. The error bars indicate the 95% confidence intervals. For this set of simulations, parameters are set to $N_p=1024$, $dt=0.001$, $t=0.8$.
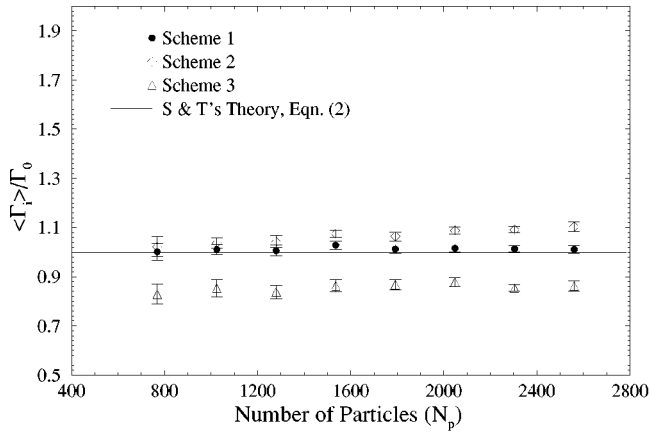
FIG. 2. Numerical collision kernels, normalized by $\Gamma_0 = 2\pi R^2 \overline{|w_r|}$, as a function of N_p. The error bars indicate the 95% confidence intervals. For this set of simulations, parameters are set to $R = 0.8 \, \Delta x$, $dt = 0.004$, $t = 0.4$.

tion of R with $N_p = 1024$. Scheme 1 with the 95% numerical confidence interval agrees with the theory for all R. Scheme 2 overestimates the collision kernel and the relative deviation increases with R. Scheme 3 underestimates the collision kernel and the relative deviation is almost independent of R. Figure 2 displays results for a fixed R but varying N_p. Similar conclusions can be drawn. In addition, the results for a new scheme, scheme 4, are given in Fig. 1. Scheme 4 is a modification to scheme 3, in which we added randomly the same number of particles that were removed due to collision. Scheme 4 may be viewed as a more realistic scheme than scheme 3 if we consider the generation of particles in the current size group as a result of collisions of smaller particles. It has the additional advantage of being stationary in the total number of particles. Interestingly, the collision kernel for scheme 4 lies in between the results of schemes 2 and 3. Furthermore, the difference between scheme 4 and scheme 2 is essentially the same as the difference between scheme 3 and the ST prediction. This may be explained by the fact that scheme 4 is essentially a combination of the requirements for scheme 2 and scheme 3. Therefore, the first three schemes we focus on here are indeed the building blocks for more complicated schemes such as scheme 4.

IV. A CRITICAL EXAMINATION OF THE SAFFMAN AND TURNER THEORY

We shall now examine the ST theory in the light of the numerical results. We first interpret the ST result in a somewhat different manner, namely, in the pure statistical sense of Gillespie.[18,19] The origin for the deviations from the theory in schemes 2 and 3 will be explored next.

A. Rephrasing the Saffman and Turner theory

Consider scheme 1, which was shown to have the same collision kernel as the ST theory. Let α be the probability that any given particle pair will collide, in the sense of the collision definition of Sec. II C 1, in the time interval between t and $t + dt$, then

$$\alpha = \Gamma \, dt / \Omega, \tag{15}$$

where Γ is the collision kernel given by Eq. (2). In fact, $\Gamma \, dt$ is the volume of fresh fluid coming into the collision zone[1] of a given particle during the time interval. If one assumes that every collision is independent,[20] then the probability of having k collisions in the time interval follows the Binomial (or Bernoulli) distribution,

$$P(k) \approx \frac{M!}{k!(M-k)!} \, \alpha^k (1-\alpha)^{M-k}, \quad \text{for } k = 0, 1, 2, \ldots, M; \tag{16}$$

where $M = N_p(N_p - 1)/2$ is the total number of possible pairs in the system. Therefore, the average number of collisions is αM with a standard deviation of $\sqrt{\alpha M}$. The average collision kernel can then be estimated as

$$\Gamma = \frac{\Omega \langle N_c(t^{(n)} \to t^{(n+1)}) \rangle}{M \, dt} = \frac{2\Omega \langle N_c(0 \to t) \rangle}{t N_p^2} = \langle \Gamma_1 \rangle. \tag{17}$$

Since only N_c is a random number and its standard deviation is $\sqrt{N_c}$, the standard deviation of the estimate Γ is

$$\sigma = \frac{\Omega \sqrt{\langle N_c(0 \to t) \rangle}}{Mt} = \frac{\Omega \sqrt{(\Gamma t M / \Omega)}}{Mt}$$
$$= \sqrt{\frac{\Gamma \Omega}{Mt}} \approx \frac{1}{N_p} \sqrt{\frac{2\Gamma \Omega}{t}}, \tag{18}$$

where t is the total integration time. Therefore we can even *predict* the uncertainty in the numerical experiment, which is inversely proportional to N_p and $t^{1/2}$ for scheme 1. This uncertainty prediction can be applied to the other two schemes as well, with N_p modified according to Eq. (9). Of significance is the observation that while single-particle statistics such as particle rms fluctuating velocity involves an uncertainty inversely proportional to $N_p^{1/2}$, the collision kernel is a two-particle statistics and the uncertainty drops more quickly with increasing N_p.

In the above interpretation, the underlying assumptions are that (a) each particle moves independent of other particles in the system and as such may overlap in space with another particle; (b) the presence of each particle is not affected by any collision event, for example, particles should not be removed from the system when a collision occurs. This is exactly our collision counting scheme 1.

The numerical uncertainties were compared with the prediction of Eq. (18) in Fig. 3 for a fixed N_p with varying R, and in Fig. 4 with different N_p. The agreement is excellent, considering that there is a significant *numerical uncertainty in the uncertainty*.

B. The deviation in scheme 2

We can now answer the question of why the counting scheme 2 gives a slightly larger collision kernel. In this scheme, the overlapping particles at the beginning of each time step are excluded from the collision detection. Let us examine what the effect is of the nonoverlapping assumption on the numerical collision kernel.

Phys. Fluids, Vol. 10, No. 1, January 1998

Wang, Wexler, and Zhou   271
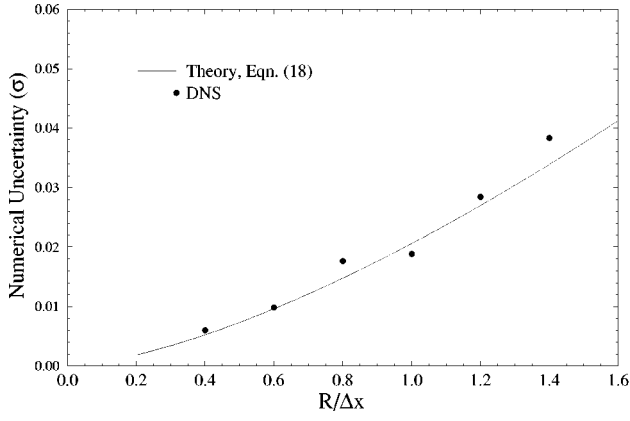
FIG. 3. Numerical standard deviation on $\langle \Gamma_1 \rangle$ as a function of collision radius R with $N_p = 1024$, $dt = 0.001$, and $t = 0.8$.

Let us first estimate analytically the value of N_0, the number of overlapping pairs in a system with N_p particles. Since any two particles will overlap if the center of the second particle is within a distance R from the center of the first particle, the probability that any two particles will overlap is $p \equiv 4\pi R^3/(3\Omega)$. All together, there are $M \equiv N_p(N_p-1)/2$ possible pairs. As a first approximation, we may assume that all the pairs are independent, so the possibility of observing k overlapping pairs, $P(k)$, again follows the Binomial distribution,

$$P(k) \approx \frac{M!}{k!(M-k)!} \, p^k (1-p)^{M-k}, \quad \text{for } k = 0,1,2,...,M;$$

(19)

and since typically, $M \gg 1$ and $p \ll 1$, this reduces to a Poisson distribution,

$$P(k) \approx \frac{\lambda^k}{k!} \, e^{-\lambda},$$

(20)

with $\lambda = pM$. Therefore, the average number of overlapping pairs is
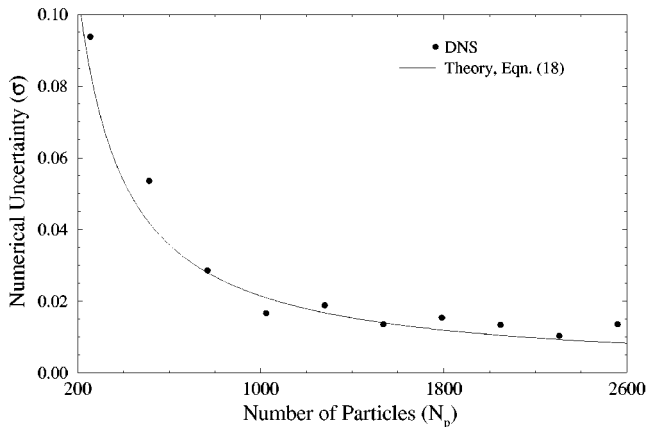
FIG. 4. Numerical standard deviation on $\langle \Gamma_1 \rangle$ as a function of N_p, with $R = 0.8 \, \Delta x$, $dt = 0.004$, and $t = 0.4$.

$$N_0 \approx pM = \frac{2\pi}{3} \, N_p(N_p-1) \, \frac{R^3}{\Omega},$$

(21)

and the standard deviation of this estimate is roughly $\sqrt{N_0}$. As an example, if $N_p = 1,024$, $\Omega = (2\pi)^3$, and $R = 0.8 \times 2\pi/32$, then $N_0 \approx 34.3 \pm 5.9$. Numerical experiments with the same number of particles show $\langle N_0 \rangle = 34.5$, which is in excellent agreement with (21).

The ratio of N_0 to N_p is easily shown to be directly proportional to the particle volume fraction, ϕ, if $N_p \gg 1$,

$$\frac{N_0}{N_p} \approx 4\phi.$$

(22)

We shall now derive an approximate relationship between $\langle \Gamma_2 \rangle$ and Γ. We note that scheme 2 considers, on average, a system of $N_p - 2N_0$ particles. The total number of possible pairs considered for collision is $M' \equiv (N_p - 2N_0) \times (N_p - 2N_0 - 1)/2$. To ease our discussion, let us separate the whole particle system into two groups. The subset of $2N_0$ overlapping particles is referred to as group A and the remaining $N_p - 2N_0$ particles are grouped into group B. First, collisions among group A particles are negligible, this includes type III collision events and type I and II collisions among group A particles. Type III collisions are negligible anyway if dt is very small. Type I and II collisions among group A particles are not significant, because the number is on the order of $N_0^2 \Gamma \, dt/\Omega$, which is of higher order, if $N_0/N_p \ll 1$, as compared to collisions between group A and group B. The possible collisions between group A particles and group B particles are not considered in scheme 2. The total number for this type of collision may be written as

$$N_c(AB) = N_0(N_p - 2N_0)[P(AB)],$$

(23)

where $P(AB)$ is the probability that any particle from group B will collide with a particle in a pair from group A. The probability for a particle in group B to collide with a pair from A is about $\langle \Gamma_2 \rangle dt/\Omega$, which could lead to two distinct values for $P(AB)$: (a) only one particle in the pair participates in the collision and $P(AB) = \langle \Gamma_2 \rangle dt/\Omega$; (b) both particles in the pair collide with the particle from group B and two collisions should be counted, which leads to $P(AB) = 2\langle \Gamma_2 \rangle dt/\Omega$. Therefore, $P(AB)$ is bounded by $\langle \Gamma_2 \rangle dt/\Omega$ and $2\langle \Gamma_2 \rangle dt/\Omega$. As an estimate we take the average $P(AB) = 1.5\langle \Gamma_2 \rangle dt/\Omega$. Substituting this into (23), we have

$$N_c(AB) = N_0(N_p - 2N_0) \, \frac{1.5\langle \Gamma_2 \rangle dt}{\Omega}.$$

(24)

Since $N_c \approx N_c(BB) + N_c(AB)$, we have

$$\frac{\Gamma N_p^2 \, dt}{2\Omega} \approx \frac{\langle \Gamma_2 \rangle (N_p - 2N_0)^2 \, dt}{2\Omega}$$

$$+ N_0(N_p - 2N_0) \, \frac{1.5\langle \Gamma_2 \rangle dt}{\Omega},$$

(25)

and it follows that

$$\langle \Gamma_2 \rangle = \Gamma \left(\frac{N_p^2}{N_p^2 - N_0 N_p - 2N_0^2} \right).$$

(26)

This expression can be simplified, if $N_0/N_p \ll 1$, to
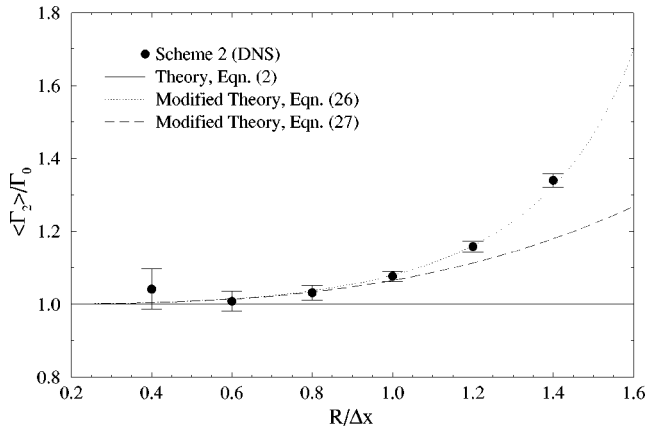
FIG. 5. Comparison of the modified theory for scheme 2 with numerical results and the Saffman and Turner theory.

FIG. 6. Ratios of local-in-time collision kernels for a typical simulation in simple shear flow.

$$\langle \Gamma_2 \rangle \approx \Gamma \left(1 + \frac{N_0}{N_p} \right) \approx \Gamma (1 + 4\phi). \tag{27}$$

This shows that the effective collision kernel for scheme 2 is larger than Γ by a factor $(1 + N_0/N_p)$, to leading order. This prediction is shown in Tables I and II and is consistent with numerical results.

The above analysis demonstrates that the ST expression does not apply to group B particles in a rigorous sense, and a system of nonoverlapping particles of a given number has slightly more collision events than a system of exactly the same size but truly randomly distributed (as in scheme 1). In Fig. 5, we replotted the numerical results for scheme 2 shown in Fig. 1, along with the modified theory, Eqs. (26) and (27). We observe an excellent agreement between Eq. (26) and the numerical results, although the expression for $P(AB)$ was not derived rigorously. The leading-order expression, Eq. (27), shows little difference from (26) for $R/\Delta x \lesssim 1.0$ or equivalently for $\phi \lesssim 1.6\%$, but underpredicts the numerical results for larger ϕ. This correction also works very well for the results of scheme 2 presented in Fig. 2.

C. The deviation in scheme 3

In scheme 3 particles are removed immediately once they collide with another particle in the system. Particles that remain in the system do not overlap (so caution is taken to eliminate those particles that overlap at $t=0$ due to random initial distribution). This scheme closely represents reality if both the collision efficiency and coagulation efficiency are close to unity, since two particles upon collision will form a particle of a larger size and as such will disappear from the current size group.

This scheme was used previously by Balachandar[2] and more recently by Hu and Mei,[9] with the expectation to match the ST prediction. However, we have demonstrated in the previous section, that the numerical collision kernel $\langle \Gamma_3 \rangle$ in *isotropic turbulence* can be much less than the ST result. Interestingly $\langle \Gamma_3 \rangle$ in the simple shear flow is similar to $\langle \Gamma_2 \rangle$ and is larger than the theory. This gives us a clue that the
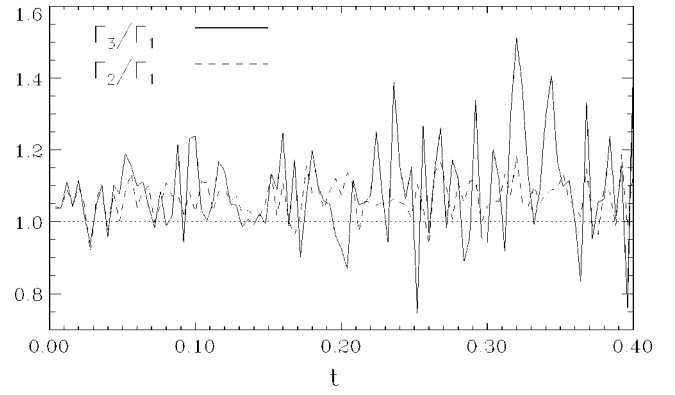
difference must be related to the nonuniform distribution or spatial variation of the local strain rate (or local dissipation rate) in turbulence, since one can imagine that the local strain rate determines the local-in-space collision kernel.

In the simple shear flow, the local straining rate is uniform. Initially uniform particle concentration will remain uniform in scheme 3, as the probability of removal is independent of spatial location, although the magnitude of concentration decreases in time. Both the removal of particles due to collisions in scheme 3 and the exclusion of nonoverlapping particles in scheme 2 have no spatial preference. We argue then that $\langle \Gamma_3 \rangle$ must be the same as $\langle \Gamma_2 \rangle$ in simple shear flow, although the numerical uncertainty in scheme 3 is larger because the removal is permanent while the overlapping in scheme 2 is not. As a consequence, the collision kernel Γ_3 in simple shear flow is a stationary random variable *in the mean*, with increasing variance in time. This is demonstrated in Fig. 6, where the local-in-time ratios Γ_3/Γ_1 and Γ_2/Γ_1 are shown for typical numerical experiments in simple shear flow, as discussed in Sec. III A. Note that for a given flow and a given initial realization of the particle system, all the collisions in a given time step using scheme 3 form a subset of the collisions in scheme 2, which again are a subset of the collisions in scheme 1. Therefore the ratios exhibit somewhat lower statistical variations than the local-in-time collision kernels.

Hu and Mei[9] also tested scheme 3 in simple shear flow, but with the expectation to match the original Smoluchowski's result given by Eq. (12). A careful examination of their results, however, indicates that the numerical collision kernel $\langle \Gamma_3 \rangle$ is slightly larger than $\Gamma_0 \equiv 4\gamma R^3/3$. For the simple shear flow one can relate $\langle \Gamma_3 \rangle$ to Γ_0 by combining Eqs. (13) and (27),

$$\langle \Gamma_3 \rangle \approx \Gamma_0 \left(1 - \frac{3\pi}{16} \frac{R}{l} \right) (1 + 4\phi). \tag{28}$$

Therefore, while the boundary correction reduces the kernel, the nonoverlapping correction increases the kernel, relative to Γ_0. In the Hu and Mei's experiment, $R/l = 0.01$ and ϕ

Phys. Fluids, Vol. 10, No. 1, January 1998

Wang, Wexler, and Zhou   273
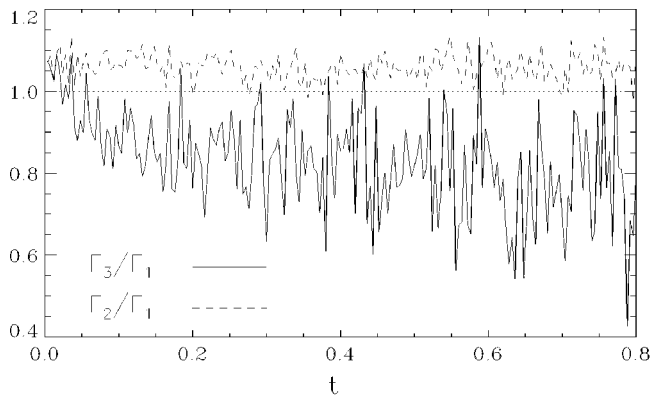
FIG. 7. Ratios of local-in-time collision kernels for the numerical experiments in the frozen turbulence shown in Table II.

$$\frac{<|\frac{\partial u}{\partial x}|+|\frac{\partial v}{\partial y}|+|\frac{\partial w}{\partial z}|>_p}{(|\frac{\partial u}{\partial x}|+|\frac{\partial v}{\partial y}|+|\frac{\partial w}{\partial z}|)}$$

$$\frac{<\epsilon>_p}{\bar{\epsilon}}$$

FIG. 8. (a) The average longitudinal strain rate and (b) the average local dissipation rate, normalized by their respective field mean, on those particles considered for collision detection as a function of time.

=0.005 24, giving $\langle \Gamma_3 \rangle \approx 1.015 \Gamma_0$. This explains why the numerical collision kernel is slightly larger than Γ_0 in their work.

Now let us return to the isotropic turbulence where the local dissipation rate is nonuniform. In addition to the correction in scheme 2, the spatial variation of the strain rate can affect the average collision kernel. In regions of high local dissipation rate collisions tend to occur more often, as the local collision rate is directly proportional to the local strain rate. Thus particles tend to be removed from the higher strain-rate regions in any time interval. For example, numerical results show that, for the scheme 3 shown in Table II, the average local strain-rate on the colliding particles is 7% larger than its field mean and the average dissipation rate is 14% larger than its field mean. For the similar case under scheme 4, numerical results show that the average local strain rate on the colliding particles is 16% larger than its field mean and the average dissipation rate is 32% larger than its field mean. Consequently, the average local strain rate seen by particles left in the system at later times must be less than the field-averaged strain rate. This effectively reduces the average numerical collision kernel. Note that this preferential removal is counteracted by turbulent advection, which tends to mix up the particles left in the flow. This implies that Γ_3 will drop initially due to the preferential removal and is *not* a stationary random variable, even in the mean. We must keep in mind that while this effect reduces the collision kernel, the nonoverlapping requirement increases it. Numerical results seem to suggest that the first effect overrides the second effect, leading to a net reduction of the collision kernel.

Figure 7 shows the local-in-time ratios, Γ_3/Γ_1, along with Γ_2/Γ_1, for the same numerical experiments shown in Table II. While Γ_2/Γ_1 is stationary, initially Γ_3/Γ_1 decreases in time quickly, followed by a slow decay in the mean at later times. At much later times, Γ_3/Γ_1 appears to level off. This is consistent with the decrease in slope of $1/N_p(t)$ versus time, evident in Balachandar[2] and Hu and Mei.[9] As a consequence, the time-averaged value $\langle \Gamma_3 \rangle$ will depend on the total integration time. Figure 7 shows that the
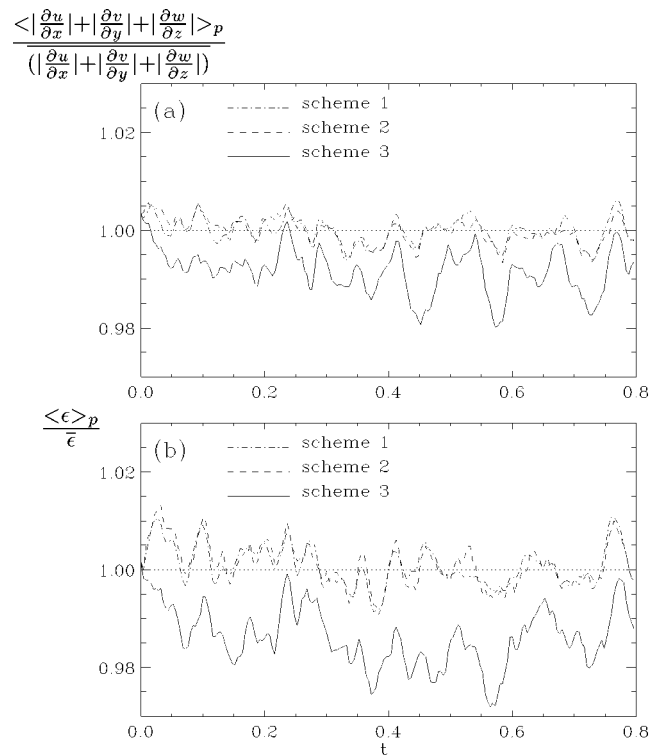
relative reduction in scheme 3 can be on average as large as 20%.

Figure 8 shows the average longitudinal strain rate and local dissipation rate, normalized by their respective field mean, seen by the particles in the system for all three schemes. No bias is observed in schemes 1 and 2, however, a small bias of about 1%–2% is clearly present in scheme 3, consistent with our speculation. There is a strong phase correlation among the three schemes as the particles in scheme 3 form a subset of the particle systems in schemes 1 and 2. Also, a phase correlation exists between the longitudinal straining rate and local dissipation rate, as the former constitutes a significant part of the latter, by definition. A loose correlation between Fig. 7 and Fig. 8 can be seen, although the data in Fig. 7 look much noisier, since collision events involve a small number of particles, while in Fig. 8 all the particles considered for the collision detection are used. The observed bias in Fig. 8 is very small, though, compared to

TABLE III. Collision kernels in evolving turbulence.

	$\langle \Gamma \rangle$	$\langle \Gamma \rangle/\Gamma$, Eq. (2)
Scheme 1	0.3911 ± 0.0042	1.008 ± 0.011
Scheme 2	0.4169 ± 0.0047	1.074 ± 0.012
Scheme 3	0.3519 ± 0.0080	0.907 ± 0.021
Eq. (2)	0.3881	...
Eq. (3)	0.4050	1.044
Eq. (27)	0.4141	1.067
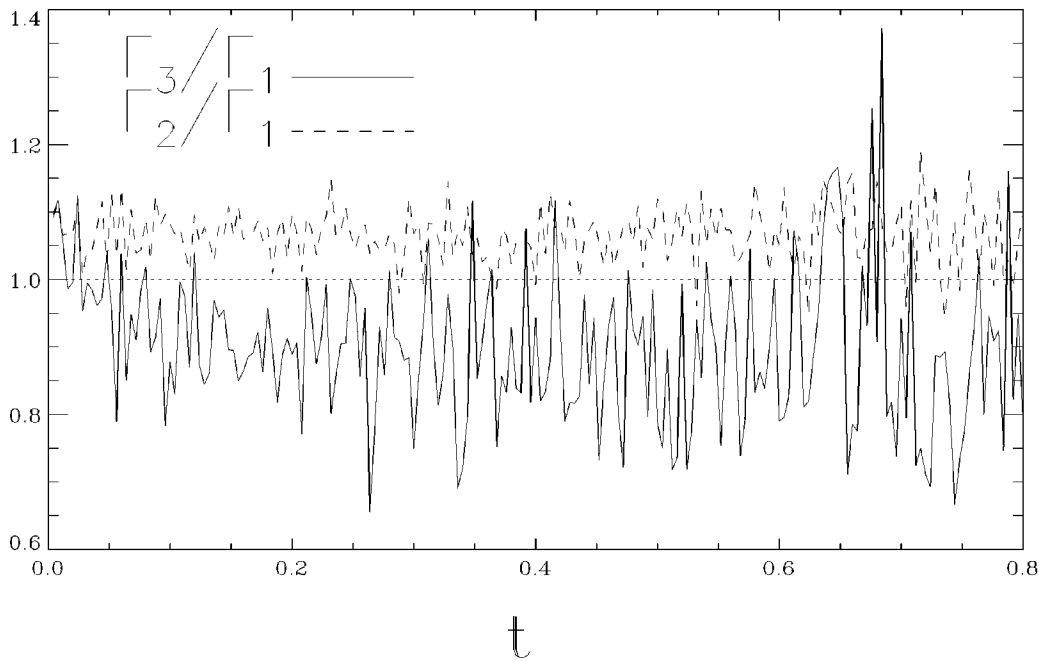
FIG. 9. Ratios of local-in-time collision kernels for the numerical experiments in the evolving turbulence shown in Table III.

the relative reduction in the collision kernel, Γ_3/Γ_1. It is not clear to us how this small bias can produce such a significant reduction or whether there is another mechanism at play. We are unable to formulate the correction in this case to the ST theory. Interestingly the average reduction, as shown in Figs. 1 and 2, is insensitive to the system parameters.

V. RESULTS FOR EVOLVING TURBULENCE

The numerical experiments considered so far used a turbulent field that did not evolve in time. Here we present results for the same parameter setting as shown in Table II but the forcing at large scales continued to be applied after the particles were introduced and collision events were counted. The flow field was exactly the same as before at $t = 0$, but was time dependent for $t > 0$. One other difference was the time step dt, which was set to 0.0004 to ensure a small CFL number for numerical stability.

Table III shows the numerical collision kernels along with the 95% numerical confidence intervals, which should be compared to the results in Table II. Since the spatially averaged relative velocity in Eq. (2) and the dissipation rate in Eq. (3) were a function of time, we further averaged them in time to give the Saffman and Turner predictions shown in Table III. We observe that the frozen and evolving flow field yield the same collision kernel for scheme 1, implying that the formulation of Saffman and Turner[1] is valid for the collision of fluid elements in an evolving flow. This should be expected since fluid elements follow the local fluid motion exactly, whether the flow is evolving or not; therefore the collision kernel is unchanged. Scheme 2 results in a collision kernel that is 7.4% larger than the prediction by Eq. (2). This relative difference is almost the same as in the frozen turbulence case, suggesting that the same correction by Eq. (26) would apply.

The collision kernel by scheme 3 is about 10% less than the prediction. Figure 9 shows the ratios of the local-in-time collision kernels as a function of time, similar to Fig. 7. Qualitatively, the behavior for $\langle\Gamma_3\rangle$ is similar as in figure 7, for the same reason as discussed in Sec. IV C. The long-time reduction of the collision kernel in scheme 3 for the evolving flow is less than in the frozen turbulence case. This should be expected, as the flow structures now move around in space with a finite lifetime, the turbulence would homogenize the particle distribution more quickly after the preferential removal due to collision. Nevertheless, the effect of biased removal cannot be overlooked.

VI. SUMMARY

Careful numerical experiments were designed to examine critically the well-known theory on the collision rate of finite-size fluid elements in isotropic turbulence developed
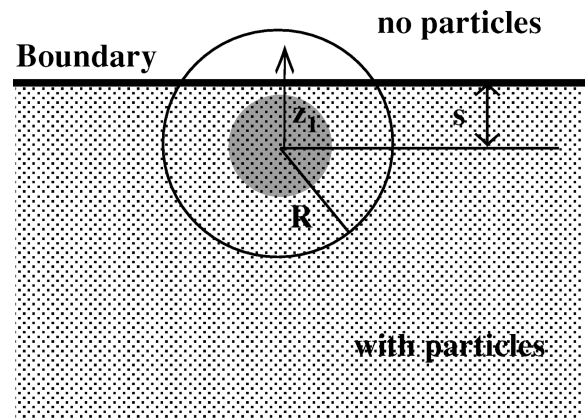
FIG. 10. A sketch to illustrate the boundary correction in simple shear flow.

by Saffman and Turner[1] over 40 yr ago. We have identified *precisely* the underlying assumptions in the ST formulation, and confirmed, for the first time, the theory with numerical simulations to within a numerical uncertainty as small as 1%.

We conclude that, rigorously speaking, the ST theory must not be exact for actual coagulation processes where particles are neither distributed independently nor kept in the same size group after collision. The nonoverlapping requirement involves a correction to the ST theory that is proportional to the particle volume fraction. The nonuniform dissipation rate in turbulence induces a biased removal that renders the particle system nonstationary. This, together with other unknown mechanisms, could result in a reduction in the collision kernel as large as 10% in an evolving turbulence and 20% in a frozen turbulence. As a consequence, care must be taken in interpreting the average collision kernel. We hope that by pointing out clearly the underlying assumptions in the Saffman and Turner theory, the exact modification to the theory for an actual coagulation process can be identified in the near future.

Although we limit the discussion to the monodisperse case, similar results are to be expected for a general particle system. The question of how the corrections can be established for a polydisperse system remains to be resolved, so is the effect of the corrections on the evolution of particle size distribution.

ACKNOWLEDGMENTS

APPENDIX: THE BOUNDARY CORRECTION OF THE COLLISION KERNEL IN SIMPLE SHEAR FLOW

The boundary correction accounts for the fact that particles near vertical boundaries (within a distance R) experience a smaller local-in-space collision kernel since no particles exist outside the domain.

Assume a particle located at a distance equal to $s(s < R)$ away from the boundary (Fig. 10), then the local collision kernel is modified to

$$\Gamma(s) = \frac{4}{3}\gamma R^3 - \int_s^R \gamma z_1 2\sqrt{R^2 - z_1^2}\,dz_1$$

$$= \frac{4}{3}\gamma R^3 - \frac{2}{3}\gamma(R^2 - s^2)^{3/2},$$

where the second term represents the volume of fluid, from outside the domain, crossing over the collision volume of the given particle. The average collision kernel for the domain should be

$$\Gamma = \frac{1}{l/2}\left(\int_0^{l/2}\frac{4}{3}\gamma R^3\,dz - \int_0^R \frac{2}{3}\gamma(R^2 - s^2)^{3/2}\,ds\right)$$

$$= \frac{4}{3}\gamma R^3\left(1 - \frac{3\pi}{16}\frac{R}{l}\right),$$

where l is the domain size in the z direction.

[1] P. G. Saffman and J. S. Turner, ''On the collision of drops in turbulent clouds,'' J. Fluid Mech. **1**, 16 (1956); also Corrigendum, **196**, 599 (1988).

[2] S. Balachandar, ''Particle coagulation in homogeneous turbulence,'' Ph.D. dissertation, Division of Engineering, Brown University, 1988.

[3] M. A. Delichatsios and R. F. Probstein, ''Coagulation in turbulent flow: Theory and experiment,'' J. Colloid Interface. Sci. **51**, 394 (1974).

[4] T. R. Camp and P. C. Stein, ''Velocity gradients and internal work in fluid motion,'' J. Boston Soc. Civil Eng. **30**, 219 (1943).

[5] M. von Smoluchowski, ''Versuch einer mathematischen theorie der koagulationskinetic kolloider losunggen,'' Z. Phys. Chem **92**, 129 (1917).

[6] Y. Zhou, A. S. Wexler, and L.-P. Wang, ''On the collision rate of small particles in isotropic turbulence. Part 2. Finite inertia case,'' *7th International Symposium on Gas–Particle Flows*, Paper FEDSM 97-3685, ASME Fluids Engineering Conference (1997). Also submitted to Phys. Fluids.

[7] V. G. Levich, *Physiochemical Hydrodynamics* (Prentice–Hall, Englewood Cliffs, NJ, 1962), p. 213.

[8] K. Higashitani, K. Yamauchi, Y. Matsuno, and G. Hosokawa, ''Turbulent coagulation of particles dispersed in a viscous fluid,'' J. Chem. Eng. Jpn. **16**, 299 (1983).

[9] C. Hu and R. Mei, ''Effect of inertia on the particle collision coefficient in Gaussian turbulence,'' the *7th International Symposium on Gas–Particle Flows*, Paper FEDSM 97-3608, ASME Fluids Engineering Conference (1997).

[10] R. Kuboi, I. Komasawa, and T. Otake, ''Collision and coalescence of dispersed drops in turbulent liquid flow,'' J. Chem. Eng. Jpn. **5**, 423 (1972).

[11] G. B. J. de Boer, G. F. M. Hoedemakers, and D. Thoenes, ''Coagulation in turbulent flow: Part I,'' Chem. Eng. Res. Des. **67**, 301 (1989); ''Coagulation in turbulent flow: Part II,'' *ibid.* **67**, 308 (1989).

[12] H. J. Pearson, I. A. Valioulis, and E. J. List, ''Monte Carlo simulation of coagulation in discrete particle-size distributions,'' J. Fluid Mech. **143**, 367 (1984).

[13] M. Chen, K. Kontomaris, and J. B. McLaughlin, ''Dispersion, growth, and deposition of coalescing aerosols in a direct numerical simulation of turbulent channel flow,'' ASME Gas–Particle Flows, FED-Vol. **228**, 1995, p. 27.

[14] S. Sundaram and L. R. Collins, ''Collision statistics in an isotropic, particle-laden turbulent suspension,'' J. Fluid Mech. **335**, 75 (1997).

[15] G. R. Ruetsch and M. R. Maxey, ''Small-scale features of vorticity and passive scalar fields in homogeneous isotropic turbulence,'' Phys. Fluids A **3**, 1587 (1991).

[16] L.-P. Wang and M. R. Maxey, ''Settling velocity and concentration distribution of heavy particles in homogeneous isotropic turbulence,'' J. Fluid Mech. **256**, 27 (1993).

[17] E. Eswaran and S. B. Pope, ''An examination of forcing in direct numerical simulations of turbulence,'' Comput. Fluids **16**, 257 (1988).

[18] D. T. Gillespie, ''The stochastic coalescence model for cloud droplet growth,'' J. Atmos. Sci. **29**, 1496 (1972).

[19] D. T. Gillespie, ''Three models for the coalescence growth of cloud drops,'' J. Atmos. Sci. **32**, 600 (1975).

[20] Rigorously this is not true since the total number of pairs $M = N_p(N_p - 1)/2$ is much larger than $3N_p$, the degree of freedom in the system, when N_p is large. However, this may be a reasonable assumption, because the actual collision number N_c is much less than N_p for a small dt.